ACS OMEGA

http://pubs.acs.org/journal/acsodf

Article

# Exploring the Multitarget Activity of Wedelolactone against Alzheimer's Disease: Insights from *In Silico* Study

Dang Xuan Du, Nguyen Huu Duy Khang,* Nguyen Huu Tri, Pham Cam Nam, and Nguyen Minh Thong*

Cite This: *ACS Omega* 2023, 8, 15031−15040

Read Online

ACCESS | Metrics & More | Article Recommendations | Supporting Information

**ABSTRACT:** In this study, Wedelolactone's multitarget activity against Alzheimer's disease was examined using density functional theory and molecular docking techniques. At physiological pH, the p$K_a$ and molar fractions have been estimated. The most likely relative rate constants of two radical scavenger mechanisms are formal hydrogen transfer in a lipid environment and single-electron transfer in a water solvent. Compared to Trolox ($k_{overall}$ = 8.96 × $10^4$ $M^{-1}$ $s^{-1}$), Wedelolactone ($k_{overall}$ = 4.26 × $10^9$ $M^{-1}$ $s^{-1}$) is more efficient in scavenging the $HOO^{\bullet}$ radical in an aqueous environment. The chelation capacity of metals was investigated by examining the complexation of the Cu(II) ion at various coordination positions and calculating the complexation kinetic constants. Furthermore, molecular docking simulations showed that the known forms of Wedelolactone at physiological pH effectively inhibited the AChE and BChE enzymes by comparing their activity to that of tacrine (control). Wedelolactone is a promising drug candidate for Alzheimer's disease therapy in light of these findings.

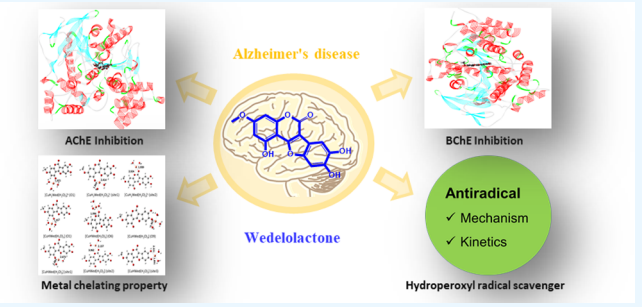


## 1. INTRODUCTION

A prevalent kind of dementia among elderly persons is Alzheimer's disease (AD). Oxidative stress is linked to the formation and progression of AD.[1,2] As people age, their antioxidant defense system gradually deteriorates. According to recent research, oxidative damage occurs before developing senile plaques and neurofibrillary tangles in the brain, two additional clinical symptoms of AD.[3−5] Moreover, the brain tissues of AD patients had abnormally high quantities of metal ions (like copper, zinc, and iron), ranging from three to six times the level found in healthy human brains.[6,7] This dyshomeostasis of metal ions is extremely important since the creation of harmful metal−amyloid complexes enhance the aggregation of amyloid $\beta$ proteins.[8] In addition, since the redox character of the metal cations concerned and the presence of oxygen molecules in brain tissue, these activities also result in the production of reactive oxygen species (ROS) via Fenton-like processes, which enhance oxidative stress. ROS damage can be prevented by increasing the number of antioxidant molecules found in the brain.[9,10]

Furthermore, the cholinergic hypothesis is the most common way to explain how AD happens and directly causes cognitive decline.[11,12] Also, it has been found that cholinesterases (ChEs) like acetylcholinesterase (AChE) and butyrylcholinesterase (BChE) can cause amyloid protein plaques and that using inhibitors can reduce these plaques. In the brains of healthy people, AChE is responsible for 80% of ChE activity, while BChE is responsible for the remaining 20%.[13] However, as AD progresses, AChE levels in the brain fall to 55−67% of normal levels while BuChE levels rise to 120% of normal levels, demonstrating that BChE is crucial for acetylcholine hydrolysis in the late stages of AD.[14,15] A change in the BChE/AChE ratio from 0.6 to as high as 1.1 can cause cholinergic deficits in these areas, leading to behavioral and cognitive problems.[16,17] Additionally, creating highly selective BChE inhibitors may help prevent some of the typical cholinergic adverse effects linked to AChE inhibition.[18] As a result, inhibiting BChE activity may prove advantageous as a treatment for AD.[19,20] Thus, drug developers are becoming interested in finding both AChE and BChE inhibitors.

Only a few drugs have been licensed to treat the disease's symptoms and enhance patients' quality of life.[21] But their clinical impact is limited due to low selectivity, low bioavailability, and unwanted side effects. Because of these factors, it is essential to develop AD research in order to comprehend the mechanisms involved in the disease's formation and the creation of new, more effective, and tailored

**Received:** December 16, 2022
**Accepted:** April 7, 2023
**Published:** April 18, 2023

ACS Publications

© 2023 The Authors. Published by American Chemical Society

medications. As a result of the many different causes of AD, a new approach to designing treatment agents for the disease is the development of multitarget medicines to be more effective in treating it.[22,23]

Using computational tools, we can anticipate a drug's effectiveness in humans, improve its pharmacokinetic features, identify new targets, and lessen its adverse effects. The "*in silico*" methodology also aids in lowering expenses and speeding up the whole design procedure.[24−26] Inspired by multifunctional design and aware of the importance of computational tools, researchers have been using computers to evaluate the therapeutic potential of new compounds that show promise as multitarget AD treatment candidates.[27−30]

Wedelolactone, a coumestan derivative generated from plants, has many valuable biological benefits, including anti-tumor[31] and anti-hepatotoxicity effects,[32] antioxidant[33] and anti-diabetic activities,[34] and anti-inflammatory properties[35] and protection of neuropharmacological functions.[36] In terms of antioxidant activity, previous studies confirmed the good radical scavenging activity of Wedelolactone[33,37] and some typical coumestan derivatives.[38,39] However, a broader analysis of the mechanism, kinetics, and all states produced by acid−base equilibria in a water solvent to evaluate the HOO$^{\bullet}$ radical scavenging ability of Wedelolactone has not been done before. When proposed as a potential molecule for creating novel therapeutics for AD treatment, a deeper understanding of Wedelolactone's structural and electrical properties and biological mechanisms is beneficial.

To understand and theoretically rationalize the mechanism of anti-AD action of Wedelolactone, density functional theory (DFT) was applied to evaluate the antiradical activity and metal-chelating characteristics, and molecular docking was used to examine the inhibition of AChE and BChE enzymes.

## 2. COMPUTATIONAL METHODS

**2.1. Quantum Chemical Calculations.** Density functional theory (DFT) methods included in the Gaussian 09 program were utilized for geometry optimization and frequency computations.[40] The M05-2X functional was chosen because its developers recommended for kinetic calculations.[41] It has been widely used for the kinetic calculation in organic and biological systems involving free radical reactions due to low errors compared with experimental data[42−44] and also among the best-performing functionals for calculating reaction energies involving free radicals.[45] In this paper, the level of theory M05-2X/6-31+G(d,p) was used for evaluating the radical scavenging activity of antioxidants because the $k_{calc.}/k_{exp.}$ ratio was estimated to be about 1−2.9[44] and has also been successfully used by other authors.[46−51] Solvation model density (SMD) method was utilized to examine the effect of pentylethanoate and water medium on the antioxidant's antiradical capability.[52] The rate constants were calculated using the QM-ORSA (quantum mechanics-based test for overall free radical scavenging activity) technique.[44,53] Table S1 given in the Supporting Information (SI) describes the procedure in further detail. Regarding species with several conformers, we examined all of them and used the conformer with the lowest electronic energy in our computations.[54]

Copper complex formation constants ($K_f$) were determined using eq 1

$$K_f = e^{-\Delta_f G^0/RT} \quad (1)$$

where $R$ denotes the gas constant, $T$ represents the temperature (298.15 K), and $\Delta_f G^0$ denotes the standard Gibbs free energy change for the complex formation reaction.

The Cartesian coordinates, standard enthalpies, and Gibbs free energies of studied structures computed in this work are shown in Table S2 of the SI.

**2.2. Molecular Docking Simulations.** From the optimized chemical structures (using the DFT method in Section 2.1), these compounds were converted into format*mdb to create the input database for the MOE docking. The structural information of the AChE (PDB ID: 1ACJ)[55] and BChE (PDB ID: 4BDS)[56] proteins were taken from the Protein Data Bank.

In order to prepare the receptor for docking studies, the three-dimensional (3D) protonation of the protein structures was set up using the Quickprep tool of MOE. The ligands were docked into the active site of the protein using the Triangular Matching docking method, and 10 different configurations were generated based on the binding free energies of each complex. The most stable molecules with the highest affinities for receptor interaction were predicted to be in poses with the lowest binding free energy. Docking simulations of the ligands toward the AChE and BChE enzymes were performed by using the MOE software. Discovery Studio was used to investigate the ligand−receptor interactions.[57]

## 3. RESULTS AND DISCUSSIONS

**3.1. Directed Antioxidant Properties.** As shown in our previous papers,[58,59] acid−base equilibria should be considered in the context of the activity in an aqueous environment that can affect the studied compound's antiradical characteristics. Three potential acidic sites, which correspond to phenolic moieties, are shown in $H_3$Wed (Figure 2). The tendency for deprotonation at these locations (see Figure 1) was estimated

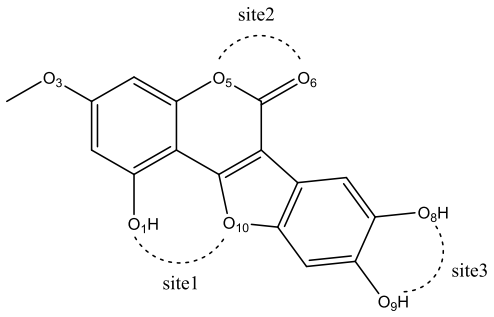


**Figure 1.** Structure of Wedelolactone ($H_3$Wed), 1,8,9-Trihydroxy-3-methoxy-6H-[1]benzofuro[3,2-*c*][1]benzopyran-6-one.

by comparing the energies of the corresponding anionic species. This investigation indicates that deprotonation can most likely take place at site $O_1H$. The $O_9H$ site was chosen as the second deprotonation site because it is the most stable dianion in the second acid−base equilibrium (see Figure 2). As far as we know, its p$K_a$ values have not been reported. Thus, the p$K_a$ of $H_3$Wed has been calculated using the isodesmic reaction and thermochemical cycles method.[60,61]

Table 1 shows the neutral ($H_3$Wed), monoanionic ($H_2$Wed$^-$), and dianionic (HWed$^{2-}$) molar fractions at physiological pH, which correspond to 0.0369, 0.4649, and 0.4982, respectively. These figures unequivocally demonstrate that the ionic species are the main form of Wedelolactone at pH = 7.4. Therefore, only monoanionic and dianionic species


https://doi.org/10.1021/acsomega.2c08014
ACS Omega 2023, 8, 15031−15040

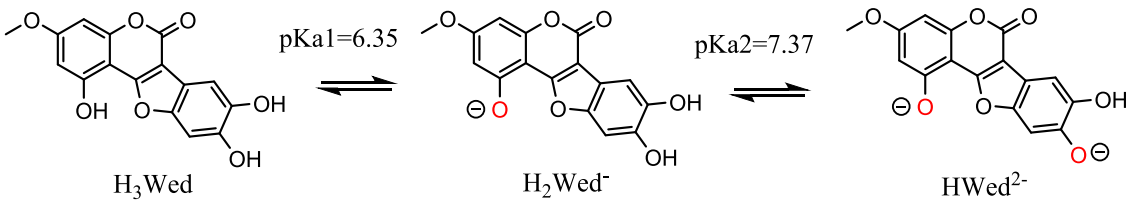


**Figure 2.** Potential deprotonation routes of Wedelolactone at physiological pH.

**Table 1. Various Acid−Base States Molar Fractions of Wedelolactone at pH = 7.4**

| species | $H_3Wed$ | $H_2Wed^-$ | $HWed^{2-}$ |
|---|---|---|---|
| f | 0.0369 | 0.4649 | 0.4982 |

were considered when simulating reactions in aqueous solution.

Peroxyl radicals ($ROO^\bullet$) are living organisms' primary molecules responsible for oxidative stress.[62] The phenolic compounds that are the most selective in deactivating peroxyl radicals due to their ability to block their harm quickly are the ideal partners for $ROO^\bullet$ radicals.[63,64] The $ROO^\bullet$ radicals are an excellent option for investigating antiradical activity because their reactivity ranges from low to moderate.[53,62] Thus, hydroperoxyl radical ($HOO^\bullet$), the smallest member of the peroxyl family, was considered the reactive oxygen species to investigate the antioxidant activity displayed through free radical scavenging.

As previously mentioned, it is crucial to include all states produced by acid−base equilibria in a water solvent to evaluate the $HOO^\bullet$ radical scavenging ability of Wedelolactone. To better understand the connection between Wedelolactone's structural characteristics and its antiradical activity, we focused on two, the formal hydro transfer (FHT) and single-electron transfer (SET), mechanisms that are important by our[58,59] and other research groups.[65,66]

- FHT (Formal Hydro Transfer)

$$H_3Wed + HOO^\cdot \rightarrow H_2Wed^\cdot + H_2O_2 \quad (2)$$

$$H_2Wed^- + HOO^\cdot \rightarrow HWed^{\cdot -} + H_2O_2 \quad (3)$$

$$HWed^{2-} + HOO^\cdot \rightarrow Wed^{2\cdot -} + H_2O_2 \quad (4)$$

- SET (Single-Electron Transfer)

$$H_2Wed^- + HOO^\cdot \rightarrow H_2Wed^\cdot + HOO^- \quad (5)$$

$$HWed^{2-} + HOO^\cdot \rightarrow HWed^{\cdot -} + HOO^- \quad (6)$$

All possible reaction routes were investigated for their thermodynamic feasibility by calculating their Gibbs free energy of reaction ($\Delta_rG^0$). Then, only exergonic reaction routes ($\Delta_rG^0 < 0$) were employed to search the involved transition state to calculate the rate constants. Because even if the endergonic channels occurred at considerable rates, the opposite reaction would still be preferred, and they will be ignored in the kinetic calculations.

As the pentylethanoate solvent (equivalent to the lipid-like environment) is unstable for ionic species, only neutral species operating via the FHT pathways (SET not included) were studied. For both polar and nonpolar solutions, the calculated $\Delta_rG^0$ values for all reaction routes are shown in Table 2.

**Table 2. Gibbs Free Energies ($\Delta_rG^0$) of the Reactions between Wedelolactone and $HOO^\bullet$ Radical in Studied Media (in kcal/mol)**

| | aqueous medium | | lipid medium |
|---|---|---|---|
| pathways | $H_2Wed^-$ | $HWed^{2-}$ | $H_3Wed$ |
| FHT, position $O_1H$ | | | 5.1 |
| FHT, position $O_8H$ | −4.57 | −14.98 | −5.0 |
| FHT, position $O_9H$ | −10.46 | | −7.3 |
| SET | 13.80 | −1.60 | |

Here, the FHT mechanism is investigated in a nonpolar solvent (pentylethanoate) containing only the $H_3Wed$ form. The results show that the capture of hydrogen atoms by the $HOO^\bullet$ at sites $O_8H$ and $O_9H$ is exergonic by −5.0 and −7.3 kcal/mol, respectively, while the capture at site $O_1H$ is slightly positive ($\Delta_rG^0$ = 5.1 kcal/mol). Alternatively, all reactions involving $H_2Wed^-$ and $HWed^{2-}$ that follow the FHT pathway in an aqueous solution are predicted to be exergonic, with $\Delta_rG^0$ values ranging from −4.57 to −14.98 kcal/mol. Optimized transition-state (TS) geometries for thermochemically feasible reaction pathways are depicted in Figure 3.

We have also investigated the potential for a SET mechanism to occur in a water solution. The Gibbs free energies of the SET processes have been determined for deprotonated species reacting with the $HOO^\bullet$ radical in water at 298.15 K. Data in Table 2 suggest that the SET mechanism is not thermodynamically feasible for the monoanionic molecule ($\Delta_rG^0$ = 13.80 kcal/mol). On the other hand, the dianion species is involved in an exergonic SET reaction ($\Delta_rG^0$ = −1.60 kcal/mol).

The total rate coefficients ($k_{total}$) and overall rate coefficients ($k_{overall}$) for the reactions in each solvent are computed and shown in Table 3. In a nonpolar solution, where only the neutral species is present, the values of $k_{total}$ and $k_{overall}$ are identical (eq 7).

In nonpolar medium:

$$k_{overall} = k_{total} = \sum k_{app}^{FHT}(H_3Wed) \quad (7)$$

In an aqueous environment at pH = 7.4, the $k_{total}$ and $k_{overall}$ values of acid−base species can be determined by applying the eqs 8−10.

In polar solution:

$$k_{total}(H_2Wed^-) = \sum k_{app}^{FHT}(H_2Wed^-) \quad (8)$$

$$k_{total}(HWed^{2-}) = \sum k_{app}^{FHT}(H_2Wed^-) + \sum k_{app}^{SET}(H_2Wed^-) \quad (9)$$

$$k_{overall} = f_{(anion)} \cdot k_{total}(H_2Wed^-) + f_{(dianion)} \cdot k_{total}(HWed^{2-}) \quad (10)$$



https://doi.org/10.1021/acsomega.2c08014
ACS Omega 2023, 8, 15031−15040

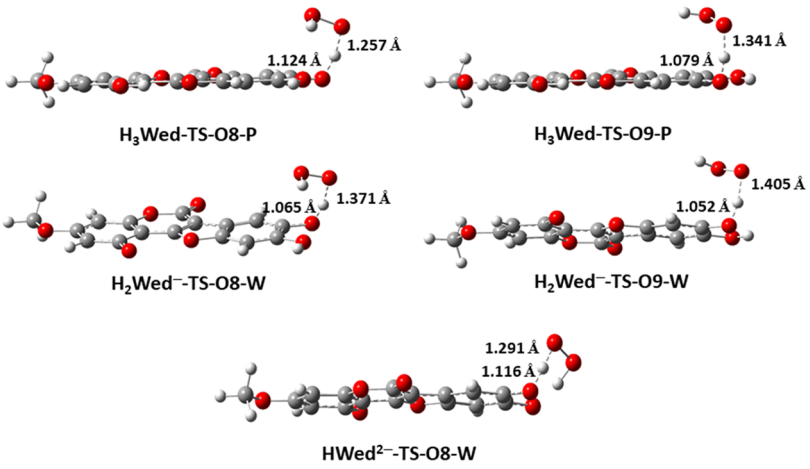


**Figure 3.** Optimized transition-state geometries of the studied species were calculated at the M05-2X/6-31+G(d,p) level. (W: water, P: pentylethanoate).

**Table 3. Calculated Rate Constant Values ($k_{app}$, $k_{total}$, and $k_{overall}$) of the Reactions of Wedelolactone with HOO• Radical (in $M^{-1}$ $s^{-1}$)**

| | $k_{app}$ in aqueous medium | | $k_{app}$ in lipid medium |
|---|---|---|---|
| channels | $H_2Wed^-$ | $HWed^{2-}$ | $H_3Wed$ |
| FHT, position $O_8H$ | $1.51 \times 10^8$ | $4.52 \times 10^9$ | $6.30 \times 10^1$ |
| FHT, position $O_9H$ | $7.36 \times 10^8$ | | $4.90 \times 10^3$ |
| SET | | $3.20 \times 10^9$ | |
| $k_{total}$ | $8.87 \times 10^8$ | $7.72 \times 10^9$ | $4.96 \times 10^3$ |
| $k_{overall}$ | $4.26 \times 10^9$ | | |

The obtained results from Table 3 indicated that the HOO• radical scavenging reactivity of Wedelolactone ($k_{overall} = 4.96 \times 10^3$ $M^{-1}$ $s^{-1}$) is slightly higher than that of Trolox ($k_{overall} = 3.40 \times 10^3$ $M^{-1}$ $s^{-1}$)[47] in a nonpolar solvent. Comparisons of total rate constant computed with the same approaches support this argument. The polarity of the solvent further increases the reactivity of Wedelolactone. The overall rate coefficient in a water environment is approximately $4.26 \times 10^9$ $M^{-1}$ $s^{-1}$. As shown, Wedelolactone's ability to scavenge hydroperoxyl radicals increases around $10^5$-fold in a polar solution compared to a nonpolar medium. These results suggest that ionic species are essential for the antiradical action of Wedelolactone. Compared to Trolox, a commonly used reference antioxidant ($k_{overall} = 8.96 \times 10^4$ $M^{-1}$ $s^{-1}$),[47] Wedelolactone is predicted to be more effective in scavenging the HOO• radical ($k_{overall} = 4.26 \times 10^9$ $M^{-1}$ $s^{-1}$) in a polar solvent.

**3.2. Copper-Chelating Properties.** The present study will focus on copper since this element is pervasive in the human body and necessary for the proper functioning of most biological systems.[67,68] Copper's role in producing reactive oxygen species,[68] especially the particularly destructive OH radical, has been linked to its function in the etiology of various neurological illnesses.[69] Additionally, it has been discovered

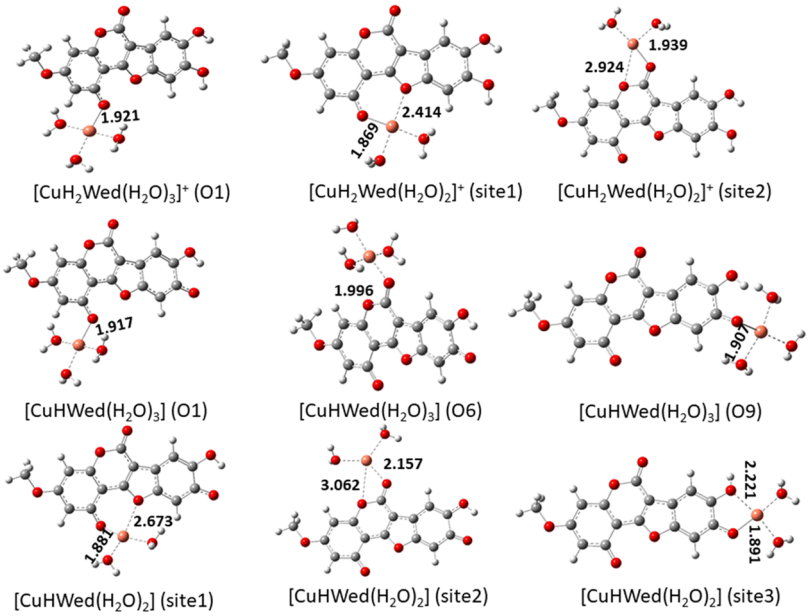


**Figure 4.** Complex structures between $[Cu(H_2O)_4]^{2+}$ and $H_2Wed^-$/$HWed^{2-}$ species involved in exergonic chelation pathways. The distances are reported in Å.



https://doi.org/10.1021/acsomega.2c08014
ACS Omega 2023, 8, 15031−15040

that Cu(II) is more harmful than Fe(III) in terms of oxidative damage under similar experimental settings.[70] Cu ions are predicted to be hydrated in the polar solution. We modeled them coordinated to water molecules. Therefore, as opposed to the bare ions, this model is more accurate in depicting "free" copper in physiological systems. For this reason, we selected a configuration including four water molecules because the most typical structure of Cu-water complexes in the aqueous medium is approximately square planar.[71,72]

At physiological pH = 7.4, the ability of Wedelolactone's acid−base equilibria to complexate $[Cu(H_2O)_4]^{2+}$ was determined by computing Gibbs free energy ($\Delta_f G^0$) for the processes listed below

$$H_2Wed^- + [Cu(H_2O)_4]^{2+} \rightarrow [CuH_2Wed(H_2O)_n]^+ + (4-n)H_2O \quad (11)$$

$$HWed^{2-} + [Cu(H_2O)_4]^{2+} \rightarrow [CuHWed(H_2O)_n] + (4-n)H_2O \quad (12)$$

The O atoms of Wedelolactone act as chelation sites in these pathways, and the Wedelolactone's potential dual role as a monodentate ($n$ = 1) and bidentate ($n$ = 2) ligand is also considered. As a result, we will look into how complexes with this geometry can form with just a single organic ligand ($H_2Wed^-$ or $HWed^{2-}$). According to the reaction described in eqs 11,12, we determined the potential formation of several complexes between $[Cu(H_2O)_4]^{2+}$ and a single $H_2Wed^-$ or $HWed^{2-}$ species. Figure 4 depicts the various structures involved in exergonic chelation pathways, and Table 4 lists the corresponding values for $\Delta_f G^0$ and $K_f$.

**Table 4. $\Delta_f G^0$, $K_f$, and $\Sigma K_f$ Values for the Various Coordinating Sites of $H_2Wed^-$ and $HWed^{2-}$**

| species | site | $\Delta_f G^0$ (kcal/mol) | $K_f$ |
|---|---|---|---|
| $H_2Wed^-$ | $O_1$ | −10.45 | $4.62 \times 10^8$ |
| | $O_3$ | 4.20 | $8.31 \times 10^{-4}$ |
| | $O_6$ | 1.34 | $1.04 \times 10^{-1}$ |
| | $O_8$ | 6.20 | $2.84 \times 10^{-5}$ |
| | $O_9$ | 7.13 | $5.90 \times 10^{-6}$ |
| | site 1 | −14.64 | $5.47 \times 10^{10}$ |
| | site 2 | −6.47 | $5.56 \times 10^4$ |
| | site 3 | 2.17 | $2.56 \times 10^{-2}$ |
| | $K^f_{total} = \Sigma K_f$ | | $5.47 \times 10^{10}$ |
| $HWed^{2-}$ | $O_1$ | −12.3 | $1.05 \times 10^9$ |
| | $O_3$ | 1.64 | $6.27 \times 10^{-2}$ |
| | $O_6$ | −2.38 | $5.57 \times 10^1$ |
| | $O_8$ | 9.85 | $5.96 \times 10^{-8}$ |
| | $O_9$ | −15.22 | $1.46 \times 10^{11}$ |
| | site 1 | −20.67 | $1.45 \times 10^{15}$ |
| | site 2 | −23.18 | $1.00 \times 10^{17}$ |
| | site 3 | −18.48 | $3.58 \times 10^{13}$ |
| | $K^f_{total} = \Sigma K_f$ | | $1.01 \times 10^{17}$ |

The $H_2Wed^-$ and $HWed^{2-}$ ligands can form monodentate complexes with the $[Cu(H_2O)_4]^{2+}$ ion at any of the seven oxygen atom locations ($O_1$, $O_3$, $O_5$, $O_6$, $O_8$, and $O_9$). Additionally, bidentate complexes are created at sites 1, 2, and 3, which are the two oxygen atom positions nearest to one another.

From Table 4, we can see that the $H_2Wed^-$ ligand prefers to coordinate at site 1, $O_1$, and site 2, with $\Delta_f G^0$ values of −14.64, −10.45, and −6.47 kcal/mol, respectively. They have $K_f$ values that range from $5.47 \times 10^{10}$ to $5.56 \times 10^4$. Concerning the $[CuH_2Wed(H_2O)_n]^+$ complexes, the Cu−$O_1$ bonds are strong because the interacting oxygen atom has a more negative charge. Cu−$O_1$ distances are 1.869 and 1.921 Å for sites 1 and $O_1$, respectively. On the other hand, the complexation reactions of $H_2Wed^-$ with $[Cu(H_2O)_4]^{2+}$ at other sites are unstable, with $\Delta_f G^0$ values that range from 1.34 to 7.13 kcal/mol and $K_f$ values that are low (vary from $1.04 \times 10^{-1}$ to $5.90 \times 10^{-6}$).

Concerning both mono and bidentate coordination modes, almost all $[CuHWed(H_2O)_n]$ complexes have noticeably high negative $\Delta_f G^0$ values (except at the $O_3$ and $O_8$ positions). These complexes are common in water because they form favorably and spontaneously and have high $K_f$ values ($5.57 \times 10^1$−$1.00 \times 10^{17}$). The Cu−O lengths for the monodentate complexes range from 1.907 to 1.996 Å, while those for the bidentate complexes are 1.881−3.062 Å (Figure 4). The obtained results reveal that $HWed^{2-}$, a dianionic ligand, was found to outperform significantly monoanionic ligands in stabilizing the produced Cu(II) complexes.

Total complex formation constants ($K^f_{total}$) were determined to be $5.47 \times 10^{10}$ for the $H_2Wed^-$ ligand and $1.01 \times 10^{17}$ for the $HWed^{2-}$ ligand, respectively, suggesting that both mono and dianionic ligands are expected to be more powerful Cu(II)-chelating agents, capable of reducing the amount of Cu(II) free ions created by the Fenton processes linked to AD.

**3.3. AChE and BChE Inhibitory Properties.** To effectively treat Alzheimer's disease, it suggests that blocking the AChE and BChE enzymes is crucial. In this section, molecular docking simulations are performed to clarify the interactions and affinities between Wedelolactone and the target enzymes AChE and BChE.

As discussed above, Wedelolactone can exist in three forms in a physiological environment: neutral ($H_3Wed$), monoanion ($H_2Wed^-$), and dianion ($HWed^{2-}$). Tacrine was used as the reference ligand for AChE and BChE, which also has two existing forms, including tacrine-neutral and tacrine-proton. Thus, these ligands' binding energies and interactions with the target proteins (AChE and BChE) were studied. Generally, only the binding site with the lowest binding energy is described in detail. The binding energy was determined as the most critical indicator in the docking studies for comparing the binding affinity of the drugs toward the targeted protein. The lower an inhibitor's docking score (DS), the stronger its binding affinity. The docking outcomes are summarized in Figures 5 and 6.

For AChE, the ligand−AChE complex's binding free energy ranged from −6.41 to −8.36 kcal/mol (Figure 5). The lowest binding free energy and highest binding affinity were found for ligand $H_3Wed$, while the highest binding free energy and lowest binding affinity were found for ligand tacrine-neutral. In the AChE-$H_3Wed$ complex, ligand $H_3Wed$ exhibits hydrogen bonding with residues Tyr130 and Tyr334, as well as non-covalent interactions with Trp84 Glu199, Phe330, Trp432, and His440 in the active site. $H_2Wed^-$ forms complexes with AChE through the following amino acids: Trp84, Ser200, Phe288, Phe290, Phe330, Phe331, Gly441, and His440. The active area of interactions in the AChE−$HWed^{2-}$ complex is covered by Trp84, Gly118, Gly119, Phe288, Phe290, Phe330, Phe331, Gly432, and His440 residues. In the case of tacrine (control),


https://doi.org/10.1021/acsomega.2c08014
ACS Omega 2023, 8, 15031−15040

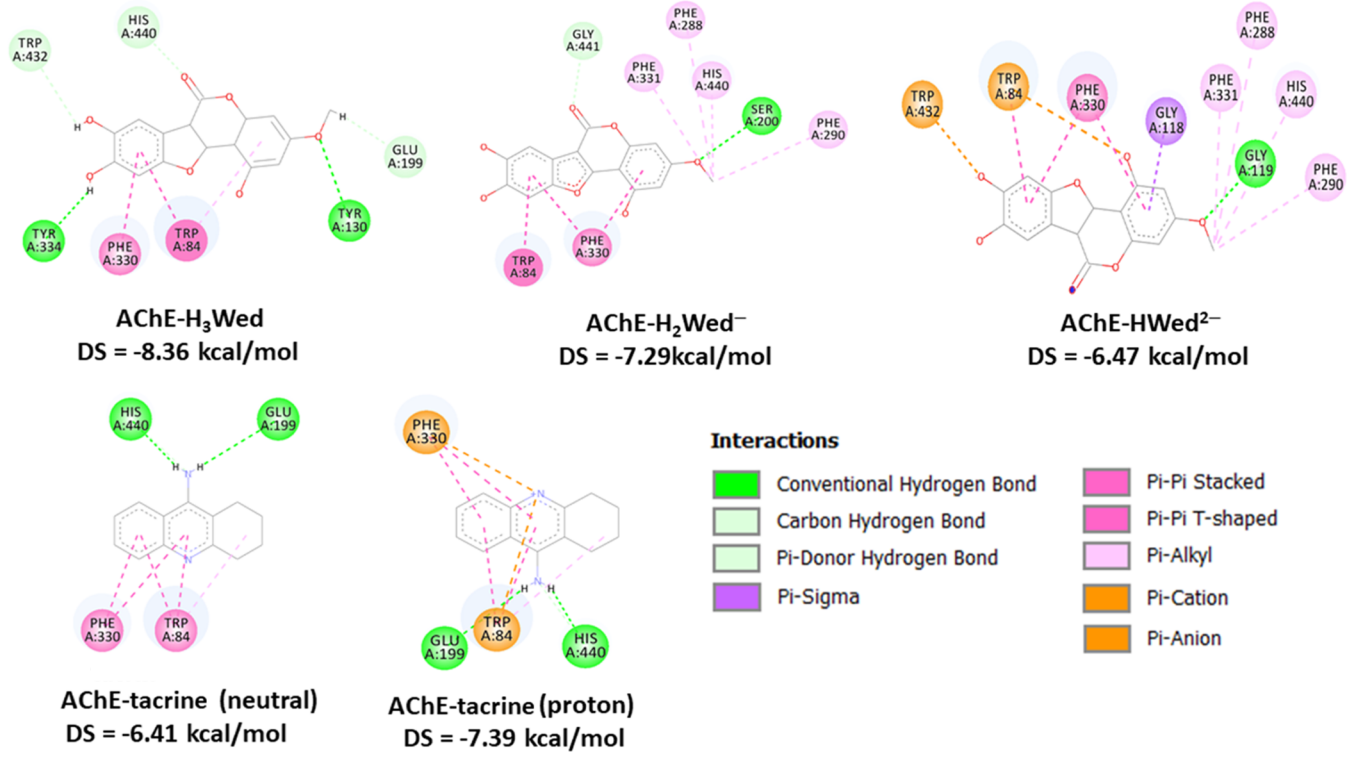


**Figure 5.** Docking score (DS) and interacting residues between ligands and AChE enzyme.

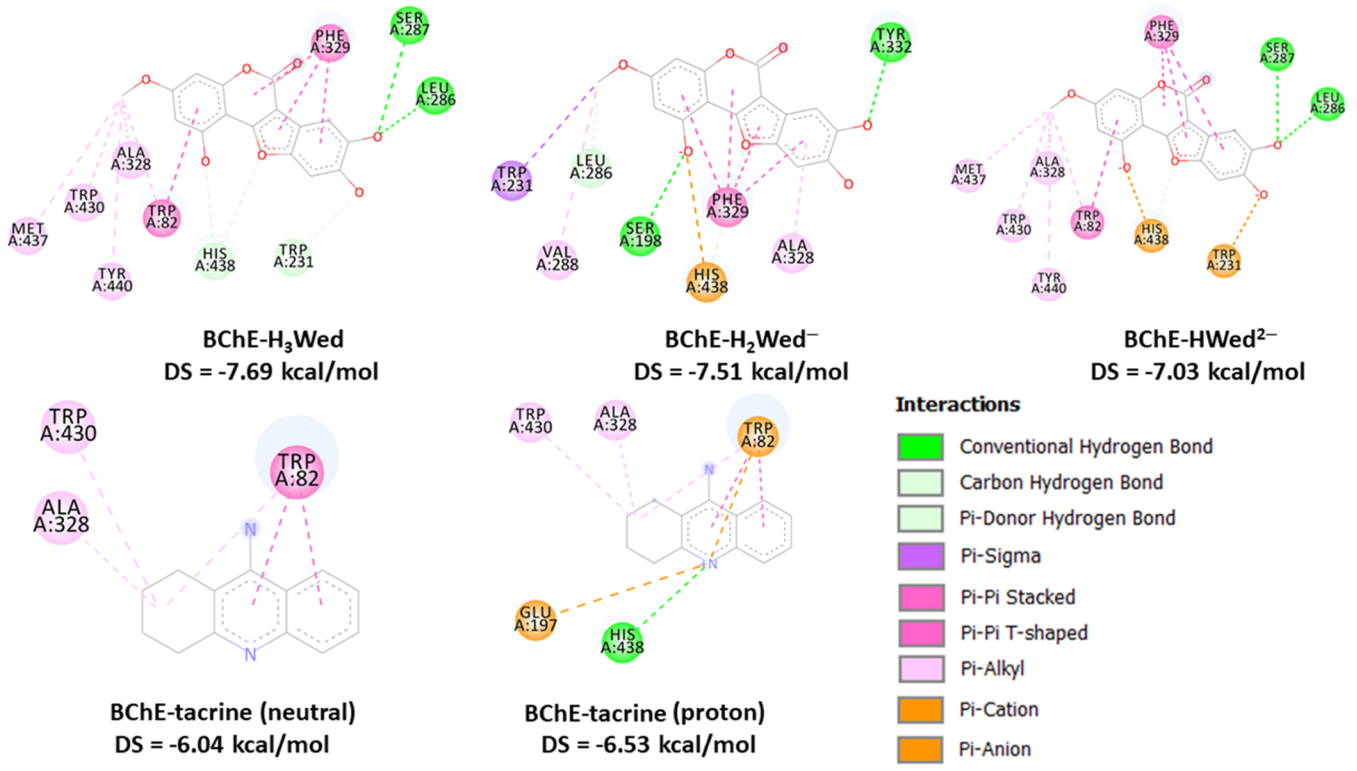


**Figure 6.** Docking score (DS) and interacting residues between ligands and BChE enzyme.

it can see interactions with amino acid residues including Trp84, Gly119, Phe330, and His440. An analysis of the AChE residues of all ligands revealed three essential residues shared by all complexes: Trp84, Phe330, and His440. These amino acids are crucial for inhibiting activity.[55,73] Therefore, Wedelolactone can be considered a potential inhibitor of the AChE enzyme.

In the case of BChE, molecular docking experiments revealed that Wedelolactone had negative binding energy values of −7.69 kcal/mol with $H_3Wed$, −7.51 kcal/mol with $H_2Wed^-$, and −7.03 kcal/mol with $HWed^{2-}$. Depending on



https://doi.org/10.1021/acsomega.2c08014
ACS Omega 2023, 8, 15031−15040

the docking score values (Figure 6), the order of these ligands' binding affinities is as follows: $H_3Wed > H_2Wed^- > HWed^{2-}$. Most notably, these values were lower than those of both tacrine-neutral (−6.04 kcal/mol) and tacrine-proton (−6.53 kcal/mol). Thus, Wedelolactone exhibited a strong binding affinity with the identified target protein comparable to the commercial drug tacrine. Figure 6 also depicts simultaneous interactions, which can shed light on the binding site interactions of the ligands for the target enzymes. $H_3Wed$ was the most effective ligand for binding to the active site of BChE by forming conventional hydrogen bonds with Leu286 and Ser287 and hydrophobic contacts with Trp82, Trp231, Ala328, Pher329, Trp430, Met437, His438, and Tyr440. In the case of the ligand $H_2Wed^-$, the interaction analysis results showed that it exhibits typical hydrogen bonds, pi−anion, pi−pi T-shaped, pi−pi stacked, and pi−alkyl contacts with BChE amino acid residues. Specifically, two hydrogen bonds were established between $H_2Wed^-$ and the residues Ser198 and Tyr332. This ligand had a pi−anion interaction with the amino acid residue His438. Furthermore, other molecular interactions interact with residues Trp231, Leu286, Val288, Ala328, and Phe329. Similarly, it was discovered that the ligand $HWed^{2-}$ interacts with the residues Leu286 and Ser287 of BChE protein through hydrogen bonds. A few other amino acid residues, including Ala328, Met437, Tyr430, and Trp440, took part in the pi−alkyl interaction. Between Trp82, Pher329, and the $HWed^{2-}$ molecule, pi−pi T-shaped and pi−pi stacked interactions were discovered. Additionally, the amino acid residues Trp231 and His438 in the active site created pi−anion interactions with the dianion molecule. Interactions between different forms of Wedelolactone and the amino acid residues Trp82, Trp231, Ser198, and His438 of the BChE enzyme were considered noteworthy since these amino acids are essential for the inhibition of activity.[74−76]

Based on the above discussion, Wedelolactone has a significant binding affinity for two target receptors. It interacts favorably with essential amino acid residues in these enzymes, suggesting it may have potential anti-Alzheimer activity.

## 4. CONCLUSIONS

In this article, the anti-Alzheimer activity of Wedelolactone is explained by computational investigations. DFT and docking molecular simulations were used to investigate the antioxidant properties as well as the AChE and BChE inhibitory activities, proposed as combined multiple target agents against AD. Our researches lead to the following conclusions:

The molar distribution shows that both mono and dianion forms predominate at physiological pH. Compared to a nonpolar medium, the ability of Wedelolactone to scavenge hydroperoxyl radical in a polar solution rises by about $10^5$. These findings point to the importance of ionic species for the antiradical effect of Wedelolactone. Compared to Trolox ($k_{overall} = 8.96 \times 10^4\ M^{-1}\ s^{-1}$), which is typically utilized as a reference antioxidant, Wedelolactone ($k_{overall} = 4.26 \times 10^9\ M^{-1}\ s^{-1}$) is more effective in the polar medium.

Taking into account the complexation's stabilization energy, the most likely of the examined complexes is the Cu(II) complex, which has the metal center coordinated to sites 1, 2, and 3 of the ligand dianion. This finding suggests that the dianionic species of Wedelolactone is a more potent Cu(II)-chelating agent, decreasing the amount of Cu(II) free ions created by the Fenton processes related to AD.

In addition, the current forms of Wedelolactone at physiological pH were demonstrated to have exceptionally good affinity with the AChE and BChE enzymes by molecular docking simulations comparing their activity to that of tacrine.

Thus, Wedelolactone is a potent therapy candidate for AD due to its multiple properties as antiradical, Cu(II) chelator, and AChE and BChE inhibitors.

## ■ ASSOCIATED CONTENT

### Supporting Information

The Supporting Information is available free of charge at https://pubs.acs.org/doi/10.1021/acsomega.2c08014.

The method to calculate rate constant following the conventional transition-state theory; the cartesian coordinates and energies of investigated structures in the studied media (PDF)

## ■ AUTHOR INFORMATION


### Corresponding Authors

**Nguyen Huu Duy Khang** − *Sai Gon University, Ho Chi Minh 700000, Vietnam*; Email: nhdkhang@sgu.edu.vn

**Nguyen Minh Thong** − *The University of Danang - Campus in Kon Tum, Kon Tum 580000, Vietnam*; orcid.org/0000-0001-9293-3876; Email: nmthong@kontum.udn.vn

### Authors

**Dang Xuan Du** − *Sai Gon University, Ho Chi Minh 700000, Vietnam*; orcid.org/0000-0002-8653-848X

**Nguyen Huu Tri** − *Sai Gon University, Ho Chi Minh 700000, Vietnam*

**Pham Cam Nam** − *The University of Danang - University of Science and Technology, Danang 550000, Vietnam*; orcid.org/0000-0002-7257-544X

Complete contact information is available at: https://pubs.acs.org/10.1021/acsomega.2c08014


### Author Contributions

D.X.D. contributed to conceptualization, investigation, methodology, and formal analysis. N.H.D.K., N.H.T. contributed to investigation, data curation, and formal analysis. P.C.N. contributed to formal analysis and writing—review & editing. N.M.T. contributed to conceptualization, investigation, methodology, formal analysis, writing—original draft.

### Notes

The authors declare no competing financial interest.

## ■ ACKNOWLEDGMENTS

This research is funded by Sai Gon University, grant no. CAS2021-06.

## ■ REFERENCES


(1) Nunomura, A.; Castellani, R. J.; Zhu, X.; Moreira, P. I.; Perry, G.; Smith, M. A. Involvement of oxidative stress in Alzheimer disease. *J. Neuropathol. Exp. Neurol.* **2006**, *65*, 631−641.

(2) Wojsiat, J.; Zoltowska, K. M.; Laskowska-Kaszub, K.; Wojda, U. Oxidant/Antioxidant Imbalance in Alzheimer's Disease: Therapeutic and Diagnostic Prospects. *Oxid. Med. Cell. Longevity* **2018**, *2018*, No. 6435861.

(3) Gu, F.; Zhu, M.; Shi, J.; Hu, Y.; Zhao, Z. Enhanced oxidative stress is an early event during development of Alzheimer-like pathologies in presenilin conditional knock-out mice. *Neurosci. Lett.* **2008**, *440*, 44−48.

(4) Moreira, P. I.; Santos, M. S.; Oliveira, C. R.; Shenk, J. C.; Nunomura, A.; Smith, M. A.; Zhu, X.; Perry, G. Alzheimer disease and the role of free radicals in the pathogenesis of the disease. *CNS Neurol. Disord.: Drug Targets* **2008**, *7*, 3−10.
(5) Goldsbury, C.; Whiteman, I. T.; Jeong, E. V.; Lim, Y. A. Oxidative stress increases levels of endogenous amyloid-beta peptides secreted from primary chick brain neurons. *Aging Cell* **2008**, *7*, 771−775.
(6) Kepp, K. P. Bioinorganic chemistry of Alzheimer's disease. *Chem. Rev.* **2012**, *112*, 5193−5239.
(7) Liu, Y.; Nguyen, M.; Robert, A.; Meunier, B. Metal Ions in Alzheimer's Disease: A Key Role or Not? *Acc. Chem. Res.* **2019**, *52*, 2026−2035.
(8) Lovell, M. A.; Robertson, J. D.; Teesdale, W. J.; Campbell, J. L.; Markesbery, W. R. Copper, iron and zinc in Alzheimer's disease senile plaques. *J. Neurol. Sci.* **1998**, *158*, 47−52.
(9) Collins, A. E.; Saleh, T. M.; Kalisch, B. E. Naturally Occurring Antioxidant Therapy in Alzheimer's Disease. *Antioxidants* **2022**, *11*, No. 213.
(10) Di Domenico, F.; Barone, E.; Perluigi, M.; Butterfield, D. A. Strategy to reduce free radical species in Alzheimer's disease: an update of selected antioxidants. *Expert Rev. Neurother.* **2015**, *15*, 19−40.
(11) Bartus, R. T. On neurodegenerative diseases, models, and treatment strategies: lessons learned and lessons forgotten a generation following the cholinergic hypothesis. *Exp. Neurol.* **2000**, *163*, 495−529.
(12) Contestabile, A. The history of the cholinergic hypothesis. *Behav. Brain Res.* **2011**, *221*, 334−340.
(13) Darvesh, S. Butyrylcholinesterase as a Diagnostic and Therapeutic Target for Alzheimer's Disease. *Curr. Alzheimer Res.* **2016**, *13*, 1173−1177.
(14) Greig, N. H.; Utsuki, T.; Yu, Q.; Zhu, X.; Holloway, H. W.; Perry, T.; Lee, B.; Ingram, D. K.; Lahiri, D. K. A new therapeutic target in Alzheimer's disease treatment: attention to butyrylcholinesterase. *Curr. Med. Res. Opin.* **2001**, *17*, 159−165.
(15) Greig, N. H.; Lahiri, D. K.; Sambamurti, K. Butyrylcholinesterase: an important new target in Alzheimer's disease therapy. *Int. Psychogeriatrics* **2002**, *14*, 77−91.
(16) Selkoe, D. J. Translating cell biology into therapeutic advances in Alzheimer's disease. *Nature* **1999**, *399*, A23−31.
(17) Li, Q.; Yang, H.; Chen, Y.; Sun, H. Recent progress in the identification of selective butyrylcholinesterase inhibitors for Alzheimer's disease. *Eur. J. Med. Chem.* **2017**, *132*, 294−309.
(18) Macdonald, I. R.; Rockwood, K.; Martin, E.; Darvesh, S. Cholinesterase inhibition in Alzheimer's disease: is specificity the answer? *J. Alzheimer's Dis.* **2014**, *42*, 379−384.
(19) Brimijoin, S.; Chen, V. P.; Pang, Y. P.; Geng, L.; Gao, Y. Physiological roles for butyrylcholinesterase: A BChE-ghrelin axis. *Chem. Biol. Interact.* **2016**, *259*, 271−275.
(20) Nordberg, A.; Ballard, C.; Bullock, R.; Darreh-Shori, T.; Somogyi, M. A review of butyrylcholinesterase as a therapeutic target in the treatment of Alzheimer's disease. *Prim. Care Companion CNS Disord.* **2013**, *15*, No. 26731.
(21) Savelieff, M. G.; Nam, G.; Kang, J.; Lee, H. J.; Lee, M.; Lim, M. H. Development of Multifunctional Molecules as Potential Therapeutic Candidates for Alzheimer's Disease, Parkinson's Disease, and Amyotrophic Lateral Sclerosis in the Last Decade. *Chem. Rev.* **2019**, *119*, 1221−1322.
(22) Oset-Gasque, M. J.; Marco-Contelles, J. Alzheimer's Disease, the "One-Molecule, One-Target" Paradigm, and the Multitarget Directed Ligand Approach. *ACS Chem. Neurosci.* **2018**, *9*, 401−403.
(23) León, R.; Garcia, A. G.; Marco-Contelles, J. Recent advances in the multitarget-directed ligands approach for the treatment of Alzheimer's disease. *Med. Res. Rev.* **2013**, *33*, 139−189.
(24) Gómez-Ganau, S.; de Julián-Ortiz, J. V.; Gozalbes, R. Recent Advances in Computational Approaches for Designing Potential Anti-Alzheimer's Agents. *Comput. Model. Drugs Against Alzheimer's Dis.* **2018**, *132*, 25−59.
(25) Baig, M. H.; Ahmad, K.; Rabbani, G.; Danishuddin, M.; Choi, I. Computer Aided Drug Design and its Application to the Development of Potential Drugs for Neurodegenerative Disorders. *Curr. Neuropharmacol.* **2018**, *16*, 740−748.
(26) Pandey, S.; Singh, B. K. De-novo Drug Design, Molecular Docking and In-Silico Molecular Prediction of AChEI Analogues through CADD Approaches as Anti-Alzheimer's Agents. *Curr. Comput.-Aided Drug Des.* **2020**, *16*, 54−72.
(27) Fernández-Bachiller, M. I.; Perez, C.; Campillo, N. E.; Paez, J. A.; Gonzalez-Munoz, G. C.; Usan, P.; Garcia-Palomero, E.; Lopez, M. G.; Villarroya, M.; Garcia, A. G.; Martinez, A.; Rodriguez-Franco, M. I. Tacrine-melatonin hybrids as multifunctional agents for Alzheimer's disease, with cholinergic, antioxidant, and neuroprotective properties. *ChemMedChem* **2009**, *4*, 828−841.
(28) Guzior, N.; Wieckowska, A.; Panek, D.; Malawska, B. Recent development of multifunctional agents as potential drug candidates for the treatment of Alzheimer's disease. *Curr. Med. Chem.* **2014**, *22*, 373−404.
(29) Hernandez-Rodriguez, M.; Correa-Basurto, J.; Martinez-Ramos, F.; Padilla, M., II; Benitez-Cardoza, C. G.; Mera-Jimenez, E.; Rosales-Hernandez, M. C. Design of multi-target compounds as AChE, BACE1, and amyloid-beta(1-42) oligomerization inhibitors: in silico and in vitro studies. *J. Alzheimer's Dis.* **2014**, *41*, 1073−1085.
(30) Martínez, A.; Zahran, M.; Gomez, M.; Cooper, C.; Guevara, J.; Ekengard, E.; Nordlander, E.; Alcendor, R.; Hambleton, S. Novel multi-target compounds in the quest for new chemotherapies against Alzheimer's disease: An experimental and theoretical study. *Bioorg. Med. Chem.* **2018**, *26*, 4823−4840.
(31) Benes, P.; Alexova, P.; Knopfova, L.; Spanova, A.; Smarda, J. Redox state alters anti-cancer effects of wedelolactone. *Environ. Mol. Mutagen.* **2012**, *53*, 515−524.
(32) Xia, Y.; Chen, J.; Cao, Y.; Xu, C.; Li, R.; Pan, Y.; Chen, X. Wedelolactone exhibits anti-fibrotic effects on human hepatic stellate cell line LX-2. *Eur. J. Pharmacol.* **2013**, *714*, 105−111.
(33) Li, X.; Wang, T.; Liu, J.; Liu, Y.; Zhang, J.; Lin, J.; Zhao, Z.; Chen, D. Effect and mechanism of wedelolactone as antioxidant-coumestan onOH-treated mesenchymal stem cells. *Arabian J. Chem.* **2020**, *13*, 184−192.
(34) Shahab, U.; Faisal, M.; Alatar, A. A.; Ahmad, S. Impact of wedelolactone in the anti-glycation and anti-diabetic activity in experimental diabetic animals. *IUBMB Life* **2018**, *70*, 547−552.
(35) Lu, Y.; Hu, D.; Ma, S.; Zhao, X.; Wang, S.; Wei, G.; Wang, X.; Wen, A.; Wang, J. Protective effect of wedelolactone against CCl4-induced acute liver injury in mice. *Int. Immunopharmacol.* **2016**, *34*, 44−52.
(36) Prakash, T.; Rao, N. R.; Swamy, A. H. Neuropharmacological studies on Wedelia calendulacea Less stem extract. *Phytomedicine* **2008**, *15*, 959−970.
(37) Chen, M.; Li, Z.; Sun, G.; Jin, S.; Hao, X.; Zhang, C.; Liu, L.; Zhang, L.; Liu, H.; Yunsheng, X. Theoretical study on the free radical scavenging potency and mechanism of natural coumestans: Roles of substituent, noncovalent interaction and solvent. *Phytochemistry* **2023**, *207*, No. 113580.
(38) Boulebd, H. Computational analysis of peroxyl radical scavenging capacity of coumestrol: insights into kinetics and reaction mechanisms. *J. Phys. Org. Chem.* **2022**, *35*, No. e4421.
(39) Djafarou, S.; Boulebd, H. The radical scavenger capacity and mechanism of prenylated coumestan-type compounds: a DFT analysis. *Free Radical Res.* **2022**, *56*, 273−281.
(40) Frisch, M. J.; Trucks, G. W.; Schlegel, H. B.; Scuseria, G. E.; Robb, M. A.; Cheeseman, J. R.; Scalmani, G.; Barone, V.; Mennucci, B.; Petersson, G. A.; Nakatsuji, H.; Caricato, M.; Li, X.; Hratchian, H. P.; Izmaylov, A. F.; Bloino, J.; Z, G.; Sonnenberg, J. L.; Hada, M.; Ehara, M.; Toyota, K.; Fukuda, R.; Hasegawa, J.; Ishida, M.; Nakajima, T.; Honda, Y.; Kitao, O.; Nakai, H.; Vreven, T.; Montgomery, J. A.; P, J. E., Jr.; Ogliaro, F.; Bearpark, M.; Heyd, J. J.; Brothers, E.; Kudin, K. N.; Staroverov, V. N.; Keith, T.; Kobayashi, R.; Normand, J.; Raghavachari, K.; Rendell, A.; Burant, J. C.; Iyengar, S. S.; Tomasi, J.; Cossi, M.; Rega, N.; Millam, J. M.; Klene, M.; Knox,


https://doi.org/10.1021/acsomega.2c08014
*ACS Omega* 2023, 8, 15031−15040

J. E.; Cross, J. B.; Bakken, V.; Adamo, C.; Jaramillo, J.; Gomperts, R.; Stratmann, R. E.; Yazyev, O.; Austin, A. J.; Cammi, R.; Pomelli, C.; Ochterski, J. W.; Martin, R. L.; Morokuma, K.; Zakrzewski, V. G.; Voth, G. A.; Salvador, P.; Dannenberg, J. J.; Dapprich, S.; Daniels, A. D.; Farkas, O.; Foresman, J. B.; Ortiz, J. V.; Cioslowski, J.; Fox, D. J. *Gaussian 09, Revision A.0*; Gaussian, Inc.: Wallingford CT, 2009.

(41) Zhao, Y.; Schultz, N. E.; Truhlar, D. G. Design of Density Functionals by Combining the Method of Constraint Satisfaction with Parametrization for Thermochemistry, Thermochemical Kinetics, and Noncovalent Interactions. *J. Chem. Theory Comput.* **2006**, *2*, 364−382.

(42) Vega-Rodriguez, A.; Alvarez-Idaboy, J. R. Quantum chemistry and TST study of the mechanisms and branching ratios for the reactions of OH with unsaturated aldehydes. *Phys. Chem. Chem. Phys.* **2009**, *11*, 7649−7658.

(43) Zavala-Oseguera, C.; Alvarez-Idaboy, J. R.; Merino, G.; Galano, A. OH radical gas phase reactions with aliphatic ethers: a variational transition state theory study. *J. Phys. Chem. A* **2009**, *113*, 13913−13920.

(44) Galano, A.; Alvarez-Idaboy, J. R. A computational methodology for accurate predictions of rate constants in solution: application to the assessment of primary antioxidant activity. *J. Comput. Chem.* **2013**, *34*, 2430−2445.

(45) Zhao, Y.; Truhlar, D. G. How well can new-generation density functionals describe the energetics of bond-dissociation reactions producing radicals? *J. Phys. Chem. A* **2008**, *112*, 1095−1099.

(46) Saïd, A. E.-h.; Mekelleche, S. M. Antioxidant activity of Trolox derivatives toward methylperoxyl radicals: thermodynamic and kinetic theoretical study. *Theor. Chem. Acc.* **2021**, *140*, No. 128.

(47) Alberto, M. E.; Russo, N.; Grand, A.; Galano, A. A physicochemical examination of the free radical scavenging activity of Trolox: mechanism, kinetics and influence of the environment. *Phys. Chem. Chem. Phys.* **2013**, *15*, 4642−4650.

(48) Alvarez-Idaboy, J. R.; Galano, A. On the chemical repair of DNA radicals by glutathione: hydrogen vs electron transfer. *J. Phys. Chem. B* **2012**, *116*, 9316−9325.

(49) Marino, T.; Galano, A.; Russo, N. Radical scavenging ability of gallic acid toward OH and OOH radicals. Reaction mechanism and rate constants from the density functional theory. *J. Phys. Chem. B* **2014**, *118*, 10380−10389.

(50) Marino, T.; Galano, A.; Mazzone, G.; Russo, N.; Alvarez-Idaboy, J. R. Chemical Insights into the Antioxidant Mechanisms of Alkylseleno and Alkyltelluro Phenols: Periodic Relatives Behaving Differently. *Chem. - Eur. J.* **2018**, *24*, 8686−8691.

(51) Galano, A.; Tan, D. X.; Reiter, R. J. On the free radical scavenging activities of melatonin's metabolites, AFMK and AMK. *J. Pineal Res.* **2013**, *54*, 245−257.

(52) Marenich, A. V.; Cramer, C. J.; Truhlar, D. G. Universal solvation model based on solute electron density and on a continuum model of the solvent defined by the bulk dielectric constant and atomic surface tensions. *J. Phys. Chem. B* **2009**, *113*, 6378−6396.

(53) Galano, A.; Raúl Alvarez-Idaboy, J. Computational strategies for predicting free radical scavengers' protection against oxidative stress: Where are we and what might follow? *Int. J. Quantum Chem.* **2018**, *119*, No. e25665.

(54) Nam, P. C.; Thong, N. M.; Hoa, N. T.; Quang, D. T.; Hoang, L. P.; Mechler, A.; Vo, Q. V. Is natural fraxin an overlooked radical scavenger? *RSC Adv.* **2021**, *11*, 14269−14275.

(55) Harel, M.; Schalk, I.; Ehret-Sabatier, L.; Bouet, F.; Goeldner, M.; Hirth, C.; Axelsen, P. H.; Silman, I.; Sussman, J. L. Quaternary ligand binding to aromatic residues in the active-site gorge of acetylcholinesterase. *Proc. Natl. Acad. Sci. U.S.A.* **1993**, *90*, 9031−9035.

(56) Nachon, F.; Carletti, E.; Ronco, C.; Trovaslet, M.; Nicolet, Y.; Jean, L.; Renard, P. Y. Crystal structures of human cholinesterases in complex with huprine W and tacrine: elements of specificity for anti-Alzheimer's drugs targeting acetyl- and butyryl-cholinesterase. *Biochem. J.* **2013**, *453*, 393−399.

(57) Biovia, D. S. *Discovery Studio Modeling Environment*; Dassault Systemes: San Diego, 2015.

(58) Cam Nam, P.; Van Bay, M.; Vo, Q. V.; Mechler, A.; Minh Thong, N. Tautomerism and antioxidant power of sulfur-benzo[h]-quinoline: DFT and molecular docking studies. *J. Mol. Liq.* **2022**, *363*, No. 119908.

(59) Quy, P. T.; Dzung, N. A.; Van Bay, M.; Van Bon, N.; Dung, D. M.; Nam, P. C.; Thong, N. M. Insights into antiradical mechanism and pro-oxidant enzyme inhibitor activity of walterolactone A/B 6-O-gallate-beta-d-pyranoglucoside originating from Euonymus laxiflorus Champ. using in silico study. *RSC Adv.* **2022**, *12*, 29975−29982.

(60) Ho, J.; Coote, M. L. First-principles prediction of acidities in the gas and solution phase. *WIREs Comput. Mol. Sci.* **2011**, *1*, 649−660.

(61) Sastre, S.; Casasnovas, R.; Muñoz, F.; Frau, J. Isodesmic reaction for pK a calculations of common organic molecules. *Theor. Chem. Acc.* **2012**, *132*, 51−58.

(62) Phaniendra, A.; Jestadi, D. B.; Periyasamy, L. Free radicals: properties, sources, targets, and their implication in various diseases. *Indian J. Clin. Biochem.* **2015**, *30*, 11−26.

(63) Leopoldini, M.; Russo, N.; Toscano, M. The molecular basis of working mechanism of natural polyphenolic antioxidants. *Food Chem.* **2011**, *125*, 288−306.

(64) Thong, N. M.; Duong, T.; Pham, L. T.; Nam, P. C. Theoretical investigation on the bond dissociation enthalpies of phenolic compounds extracted from Artocarpus altilis using ONIOM-(ROB3LYP/6-311++G(2df,2p):PM6) method. *Chem. Phys. Lett.* **2014**, *613*, 139−145.

(65) Medina, M. E.; Galano, A.; Alvarez-Idaboy, J. R. Theoretical study on the peroxyl radicals scavenging activity of esculetin and its regeneration in aqueous solution. *Phys. Chem. Chem. Phys.* **2014**, *16*, 1197−1207.

(66) León-Carmona, J. R.; Alvarez-Idaboy, J. R.; Galano, A. On the peroxyl scavenging activity of hydroxycinnamic acid derivatives: mechanisms, kinetics, and importance of the acid-base equilibrium. *Phys. Chem. Chem. Phys.* **2012**, *14*, 12534−12543.

(67) Wang, P.; Yuan, Y.; Xu, K.; Zhong, H.; Yang, Y.; Jin, S.; Yang, K.; Qi, X. Biological applications of copper-containing materials. *Bioact. Mater.* **2021**, *6*, 916−927.

(68) Gaetke, L. M.; Chow-Johnson, H. S.; Chow, C. K. Copper: toxicological relevance and mechanisms. *Arch. Toxicol.* **2014**, *88*, 1929−1938.

(69) Brewer, G. J. The risks of copper toxicity contributing to cognitive decline in the aging population and to Alzheimer's disease. *J. Am. Coll. Nutr.* **2009**, *28*, 238−242.

(70) Letelier, M. E.; Sanchez-Jofre, S.; Peredo-Silva, L.; Cortes-Troncoso, J.; Aracena-Parks, P. Mechanisms underlying iron and copper ions toxicity in biological systems: Pro-oxidant activity and protein-binding effects. *Chem.-Biol. Interact.* **2010**, *188*, 220−227.

(71) Bryantsev, V. S.; Diallo, M. S.; Goddard, W. A., 3rd Computational study of copper(II) complexation and hydrolysis in aqueous solutions using mixed cluster/continuum models. *J. Phys. Chem. A* **2009**, *113*, 9559−9567.

(72) Galano, A.; Francisco Marquez, M.; Perez-Gonzalez, A. Ellagic acid: an unusually versatile protector against oxidative stress. *Chem. Res. Toxicol.* **2014**, *27*, 904−918.

(73) Anbarani, H. M.; Pordel, M.; Bozorgmehr, M. R. Interaction of Imidazo[4,5-a]Acridines with Acetylcholinesterase. *Pharm. Chem. J.* **2022**, *56*, 762−768.

(74) Wandhammer, M.; de Koning, M.; van Grol, M.; Loiodice, M.; Saurel, L.; Noort, D.; Goeldner, M.; Nachon, F. A step toward the reactivation of aged cholinesterases–crystal structure of ligands binding to aged human butyrylcholinesterase. *Chem. Biol. Interact.* **2013**, *203*, 19−23.

(75) Nicolet, Y.; Lockridge, O.; Masson, P.; Fontecilla-Camps, J. C.; Nachon, F. Crystal Structure of Human Butyrylcholinesterase and of Its Complexes with Substrate and Products. *J. Biol. Chem.* **2003**, *278*, 41141−41147.

(76) Brus, B.; Kosak, U.; Turk, S.; Pislar, A.; Coquelle, N.; Kos, J.; Stojan, J.; Colletier, J. P.; Gobec, S. Discovery, biological evaluation,



https://doi.org/10.1021/acsomega.2c08014
*ACS Omega* 2023, 8, 15031−15040

and crystal structure of a novel nanomolar selective butyrylcholinesterase inhibitor. *J. Med. Chem.* **2014**, *57*, 8167−8179.



https://doi.org/10.1021/acsomega.2c08014
*ACS Omega* 2023, 8, 15031−15040